Published in Tectonophysics 278, issues 1-4, 31-45, 1997
which should be used for any reference to this work

Nd, Sr, and Pb isotopic evidence for diverse lithospheric mantle sources of East African Rift carbonatites

A. Kalt [a,*], E. Hegner [b], M. Satir [b]

[a] *Mineralogisches Institut, Universität Heidelberg, Im Neuenheimer Feld 236, D-69120 Heidelberg, Germany*
[b] *Institut für Mineralogie, Petrologie und Geochemie, Universität Tübingen, Wilhelmstr. 56, D-72074 Tübingen, Germany*

Abstract

Carbonatites may provide valuable information on mantle source compositions as their isotopic ratios are insensitive to crustal contamination. In order to place constraints on mantle sources, nineteen samples from three Miocene to Quaternary carbonatite areas in the East African Rift were analysed for their Sr, Nd, and Pb isotopic compositions. The samples from Kerimasi (northern Tanzania), Homa Mountain, and Wasaki Peninsula (both Lake Victoria, Kenya) as a whole show considerable variations in their isotope ratios (0.70327–0.70502 for $^{87}Sr/^{86}Sr$, 0.51249–0.51283 for $^{143}Nd/^{144}Nd$, 18.72–20.41 for $^{206}Pb/^{204}Pb$, 15.52–15.78 for $^{207}Pb/^{204}Pb$, and 39.22–40.47 for $^{208}Pb/^{204}Pb$) that lie between the inferred compositions for HIMU (high $^{238}U/^{204}Pb$ mantle) and EM I (enriched mantle I) components in most isotope plots. The internal isotopic variations of the three carbonatite areas define distinct arrays and diverse trends in isotope diagrams. Although the isotope data define linear arrays in Sr–Nd and Pb–Pb diagrams, which suggest binary mixing between HIMU and EM I mantle components, neither the isotopic compositions of the carbonatites as a whole nor the compositional ranges for individual carbonatite occurrences can be explained by such a process. This clearly emerges from the absence of linear data trends in Sr–Pb and Nd–Pb isotope plots and from the lack of consistent endmember compositions. These features are also displayed by previously published isotope data for East African carbonatites. It is therefore suggested that carbonatite complexes within the East African Rift have isotopically distinct and small mantle sources that are probably not adequately described in terms of the mantle components defined for oceanic basalts. Most likely, these sources are located in a heterogeneous lithospheric mantle and were produced by enrichment and depletion processes at different times and degrees.

Keywords: carbonatite; East African Rift; Nd–Sr–Pb isotope ratios; mantle reservoirs

1. Introduction

Carbonatites are mantle-derived magmatic rocks commonly found within rift systems and frequently associated with ijolites and melilitites. They can provide valuable information on the composition of the mantle beneath a rift as their isotopic ratios, inherited from the mantle source, are buffered against crustal contamination. This is due to: (1) very high Sr and Nd concentrations (Bell and Blenkinsop, 1989); (2) low solidus and liquidus temperatures compared to most mantle- and crustal-derived rocks (for a review see Wyllie, 1989); (3) low viscosities (Treiman, 1989); and (4) rapid ascent to the surface (Williams et al., 1986).

Approximately half of the known carbonatite occurrences world-wide are found within Africa, the majority being younger than 200 Ma and associated

* Corresponding author. Fax: +49-6221-564805.

with the East African Rift system (Woolley, 1989). Isotope studies of East African carbonatites indicate very heterogeneous mantle sources (Lancelot and Allègre, 1974; Bell and Blenkinsop, 1987; Nelson et al., 1988). Bell and Blenkinsop (1987) found data for East African carbonatites with ages between 0 and 113 Ma to correlate in a linear way on an ϵ_{Nd} versus ϵ_{Sr} diagram (EACL: East African Carbonatite Line, Fig. 2), suggesting a mixing process. For oceanic island basalts (OIB), mixing processes are generally discussed in the context of hypothetical endmembers (DMM: depleted MORB (mid-ocean ridge basalt) mantle; HIMU: high $^{238}U/^{204}Pb$ mantle; EM I: enriched mantle I; EM II: enriched mantle II; Zindler and Hart, 1986). Due to similar variations in Sr, Nd, and Pb isotopic compositions between carbonatites and basalts from oceanic islands (Lancelot and Allègre, 1974; Bell and Blenkinsop, 1987; Nelson et al., 1988; Dawson et al., 1995), mantle sources for carbonatites are also commonly interpreted in the context of these mantle components (Bell and Blenkinsop, 1987; Nelson et al., 1988; Hoernle and Tilton, 1991; Simonetti et al., 1995). As the EACL is similar in slope to the Lo–Nd line of Hart et al. (1986) in a Sr–Nd isotope diagram, the former was interpreted as a binary mixing line between HIMU and EM I mantle components (Bell, 1994). Further Sr–Nd and additional Pb isotope studies of East African carbonatites and related rocks with ages up to 126 Ma were in line with this linear correlation (Nelson et al., 1988; Kwon et al., 1989, citing unpublished data of Bell and Tilton; Keller and Krafft, 1990; Bell and Peterson, 1991; Simonetti and Bell, 1993, 1994a,b; Tilton and Bell, 1994, citing unpublished data of Bell and Tilton; Bell and Dawson, 1995; Dawson et al., 1995). On these grounds, it was concluded that the isotope data for most carbonatites younger than 200 Ma, including those from East Africa, are best interpreted as mixtures between two mantle components with isotope characteristics similar to HIMU and EM I (Bell, 1994; Tilton and Bell, 1994; Bell and Dawson, 1995).

The internal Sr–Nd–Pb isotopic variations of individual carbonatite-bearing complexes in the East African Rift, however, have been documented in only a few cases (Bell and Peterson, 1991; Simonetti and Bell, 1993, 1994a,b; Bell and Simonetti, 1996), and most of the isotopic variations in these magmatic complexes are displayed by nephelinites and other silicate magmatic rocks rather than by carbonatites. Moreover, the assumption of a mixing model to explain the isotopic variations in East African carbonatites bears several problems. Modelling magma generation with pre-defined mantle components implies that the latter are continuously available in a physical or chemical sense. It is questionable whether this applies to continental settings (Perry et al., 1987; Paslick et al., 1995; Volker et al., 1995), such as the East African Rift. For nephelinites, alkali basalts, and carbonatites from the Tanzanian part of the East African Rift, Paslick et al. (1995) found the magmas to have predominantly acquired their Sr, Nd, and Pb in the lithospheric mantle. The isotopic variations of the volcanics could not be explained by mixing of the mantle components identified in oceanic basalts. Furthermore, carbonatite magmatism requires unusual mantle compositions (Wallace and Green, 1988; Eggler, 1989; Wyllie, 1989; Sweeny, 1994). The very small volumes of carbonatites compared to the amount of silicate mantle-derived rocks in general indicate that these mantle compositions are not commonly available.

We have analysed Nd, Sr, and Pb isotopic compositions of Miocene to Quaternary carbonatites and genetically related rocks from the Kenya Rift in order to obtain more detailed information on mantle sources. We have further confined the study to carbonatites and to very few silicate rocks (ijolites and melilitites) for which a genetic relationship with carbonatites is indicated by field evidence. Nephelinitic rocks that are commonly 'associated' with carbonatites (Le Bas, 1987) are not considered here as the genetic relationship between silicate and carbonatite magmas in general is not clear (for a review see Bailey, 1993). Moreover, field relations in the Wasaki Peninsula and in the Homa Mountain area (see Section 2) indicate a spatial and temporal coincidence of nephelinite and carbonatite volcanism but not necessarily a genetic link between the two. Consequently, only carbonatite data have been considered for comparison in the discussion.

2. Geological setting and samples

The East African Rift system extends from the Afar triple junction in the north to the Zambesi

River in southern Africa. There is a distinct bifurcation north of the Tanzania Craton in Uganda, splitting the rift system into a western branch (Albert Rift, Tanganyika Rift) and an eastern branch (Kenya Rift). The eastern branch, cutting through Kenya and northern Tanzania, represents an initial stage of continental breakup. Volcanic activity started in northern Kenya in the Late Oligocene (McDougall and Watkins, 1988) and propagated southward with time. Geophysical studies (Ebinger et al., 1989; Achauer et al., 1994) as well as stratigraphic and structural constraints (Smith, 1994) support a mainly active mode of rifting driven by a mantle plume. Chemical and isotopic compositions of rift-related basaltic rocks and basanites (Class et al., 1994; Volker et al., 1995) are consistent with the presence of a mantle plume underneath northern Kenya. They further reveal interaction of the plume material with lithospheric mantle (Class et al., 1994), with asthenospheric MORB-type mantle (mid-ocean ridge basalt) and with low-temperature melting domains of EM I-type in the thermal boundary layer (Volker et al., 1995).

The samples used in this study were collected from two regions: the shores of Lake Victoria, Kenya, and Kerimasi volcano, northern Tanzania (Fig. 1). The Lake Victoria region forms part of the Kavirondo branch of the Kenya Rift (Fig. 1). Magmatism is of Miocene to Pliocene age (Baker, 1987). It produced predominantly nephelinites along with minor carbonatites as well as late phonolitic nephelinites and phonolites (McCall, 1958). The Tertiary magmatic rocks intruded and extruded onto Precambrian basement of the Tanzania Craton (Shackleton, 1993). The nephelinites (Kisingiri Volcanic Group, McCall, 1958) form deeply eroded flows and minor agglomerates, whereas the late-stage phonolitic nephelinites and phonolites form isolated plugs. Within the Lake Victoria region, there are two separate areas containing carbonatite complexes. The area northeast of Homa Bay, referred to as Homa Mountain area, comprises the Homa Mountain carbonatite centre as well as several other distinct carbonatite plugs (Fig. 1). The area west and northwest of Homa Bay, referred to as Wasaki Peninsula, comprises the complexes of Okuge, Usaki, Sokolo, South Ruri and North Ruri (Fig. 1) and other smaller carbonatite plugs. The complexes consist of intrusive carbonatites, carbonatite breccia or agglomerates, melilitites and ijolites. Carbonatite complexes and Kisingiri nephelinites form isolated outcrops (Fig. 1) but age determinations point to a roughly contemporaneous formation. The Kisingiri volcanic series probably formed between 22 and 16 Ma as inferred from Lower Miocene fossil assemblages intercalated with Kisingiri porphyroclastics and from K–Ar age determinations on whole rock and biotite (for a review see Baker et al., 1970). An age of 13 Ma for a phlogopite from a carbonatite sample of Homa Mountain (Bell and Blenkinsop, 1987) probably marks the onset of carbonatitic activity in the Kavirondo Rift.

The Kerimasi volcano in northern Tanzania straddles the western fault scarp of the Kenya Rift. It rests on Neogene lavas flooring the rift (Dawson, 1992). The volcano is younger than the major faulting phase at 1.2 Ma and has been displaced by later faulting at 0.37 Ma B.P. (Dawson, 1992). It consists of carbonatite and nephelinite pyroclastics and flows (Keller and Spettel, 1995). An age of 0.5 Ma is given for the Kerimasi by Paslick et al. (1995).

Altogether, nineteen samples were collected and analysed (Table 1). In the Lake Victoria region, samples were taken from the Homa Mountain area and from the complexes of Okuge, Usaki, Sokolo, South Ruri and North Ruri (all Wasaki Peninsula, Fig. 1). From each distinct carbonatite complex at least two samples (except for North Ruri, Wasaki Peninsula) were selected for Sr, Nd, and Pb isotopic analysis. The study is restricted to very young carbonatites (<13 Ma) so that in-situ decay is negligible due to very low parent/daughter ratios.

3. Methods and results

Sr, Nd, and Pb isotopic compositions were determined on whole rock powders. The samples were decomposed in Teflon screw-top vials in HF-$HClO_4$ for Sr and Nd isotope analyses and in HF-HNO_3 for Pb isotope analyses. For Sr and Nd isotope analyses, the samples were processed by conventional ion-exchange technique. Pb was separated employing a HBr–HCl wash and elution procedure. Total procedure blanks were less than 200 pg for Sr, less than 30 pg for Nd, and less than 100 pg for Pb. A detailed description of the analytical procedures is given in

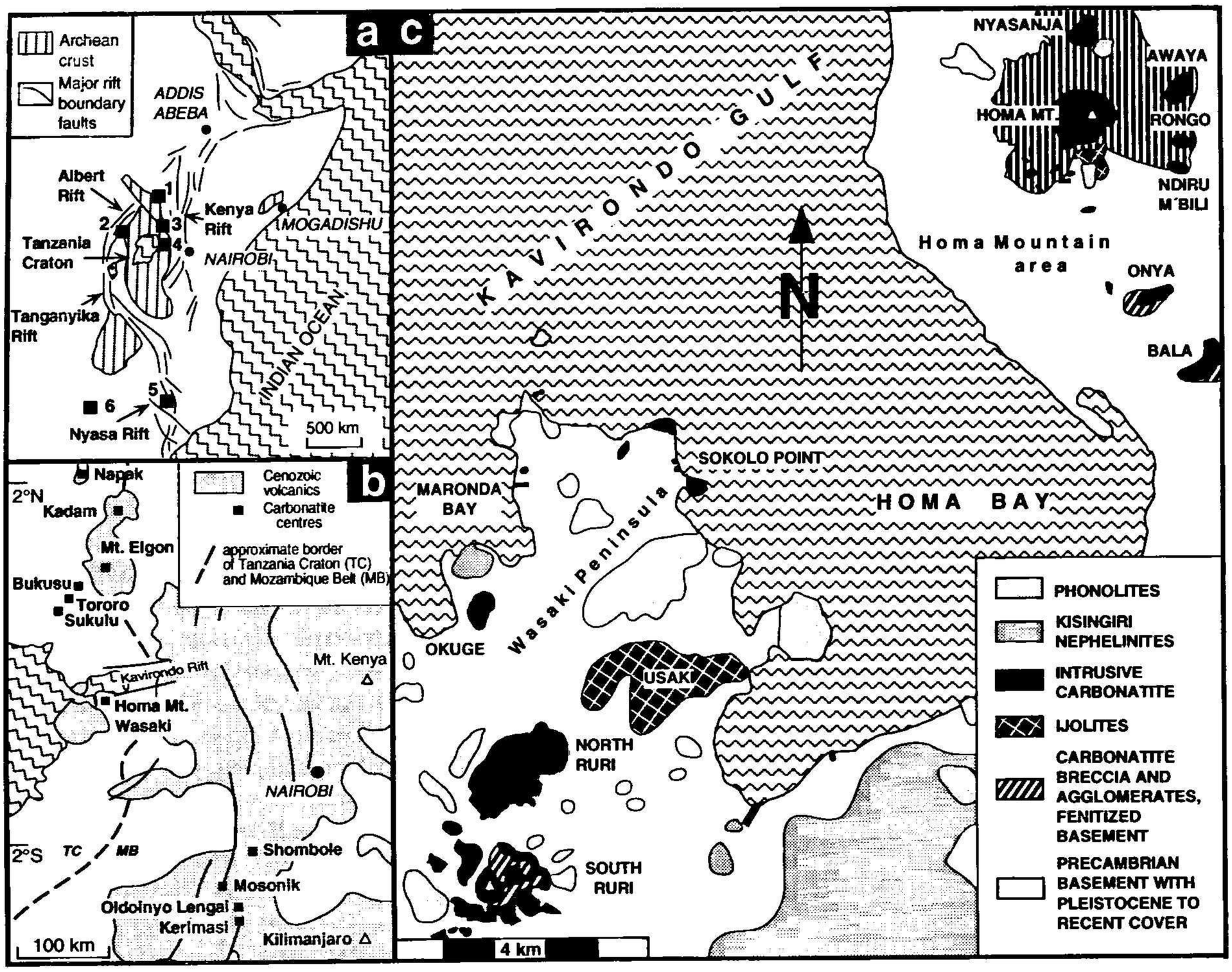

Fig. 1. (a) Simplified tectonic map of the East African Rift system, modified after Smith and Mosley (1993) and Shackleton (1993), with approximate locations of the carbonatite occurrences considered in this study. *1* = Napak (E-Uganda), *2* = Kalyango, Rusekere (W-Uganda), *3* = Bukusu, Tororo, Sukulu (E-Uganda), *4* = Homa Mountain area and Wasaki Peninsula (Lake Victoria, Kenya), *5* = Kangankunde, Chilwa (Malawi), *6* = Rufunsa (Zambia). (b) Simplified geological map of the Kenya Rift and adjacent areas in western Kenya, eastern Uganda, and northern Tanzania, modified after Dawson and Smith (1988) and Peterson (1989), with carbonatite locations. (c) Geological sketch map of the Homa Mountain area and Wasaki Peninsula, Lake Victoria, modified after McCall (1958) and Le Bas (1977).

Hegner et al. (1995). Isotope ratios were determined on a Finnigan-MAT 262 multicollector mass spectrometer employing a static collection mode for Sr and Pb and a dynamic multiple mass collection routine for Nd. Values for Nd, Sr, and Pb standards and analytical precision are included in Table 1.

Measured $^{87}Sr/^{86}Sr$ ratios for the nineteen samples range from 0.70327 to 0.70502 and measured $^{143}Nd/^{144}Nd$ ratios from 0.51249 to 0.51283 (Table 1). As all samples are between 0.37 Ma and 13 Ma old, age corrections are negligible. Calculated initial ratios for 13 Ma, assuming $^{87}Rb/^{86}Sr$ ratios between 0.0004 and 0.07 and $^{147}Sm/^{144}Nd$ ratios from 0.04 to 0.15 (Nelson et al., 1988; Ziegler, 1992), do not deviate from measured ratios within external precision (Table 1).

In a $^{143}Nd/^{144}Nd$ versus $^{87}Sr/^{86}Sr$ diagram, the measured ratios of samples from Lake Victoria and Kerimasi form an inversely correlated array (Figs. 2 and 5). Except for one sample from the Homa Mountain area (1434, Table 1), all data points plot within the upper left (depleted) quadrant of the diagram (Fig. 2).

Table 1
Sr, Nd, and Pb isotopic data for Kerimasi, Homa Mountain area and Wasaki Peninsula

Sample	Occurrence	Rock type	$^{87}Sr/^{86}Sr$	$^{143}Nd/^{144}Nd$	$^{206}Pb/^{204}Pb$	$^{207}Pb/^{204}Pb$	$^{208}Pb/^{204}Pb$
Tanzania							
TK-12	Kerimasi	carbonatite	0.703913	0.512729	20.817	15.784	40.474
TK-14	Kerimasi	carbonatite	0.703911	0.512725	20.848	15.777	40.462
TK-26	Kerimasi	carbonatite	0.704059	0.512717	20.648	15.740	40.318
Homa Mountain area							
HB-19	Homa Mt.	ol–melilitite	0.703266	0.512827	20.165	15.688	39.825
HO-1	Homa Mt.	carbonatite	0.703486	0.512763	20.414	15.719	40.253
1434	Ndiru Mbili	carbonatite	0.705015	0.512486	18.718	15.516	39.026
1423	Bala Gully	carbonatite	0.704362	0.512642	20.256	15.720	39.961
1426	Bala Gully	carbonatite	0.704156	0.512705	20.216	15.713	39.989
Wasaki Peninsula							
HO-4	Okuge	carbonatite	0.704073	0.512679	20.052	15.694	39.689
1472	Okuge	carbonatite	0.703895	0.512729	20.174	15.716	39.845
1473	Okuge	carbonatite	0.703959	0.512721	20.218	15.709	39.870
1438	Usaki	ijolite	0.703930	0.512663	19.720	15.653	39.457
1443	Usaki	ijolite	0.703987	0.512666	19.879	15.657	39.511
1448	Sokolo Point	carbonatite	0.703806	0.512708	20.257	15.694	39.957
1453	Sokolo Point	carbonatite	0.703845	0.512675	20.303	15.732	40.070
1464	South Ruri	carbonatite	0.703958	0.512743	20.343	15.711	39.895
1465	South Ruri	carbonatite	0.703979	0.512737	20.221	15.708	39.910
HB-30	South Ruri	carbonatite	0.703872	0.512679	19.272	15.607	39.220
1513	North Ruri	carbonatite	0.704173	0.512689	20.058	15.748	39.770

$^{87}Sr/^{86}Sr$ ratios are normalized to $^{86}Sr/^{88}Sr = 0.1194$, $^{143}Nd/^{144}Nd$ ratios are normalized to $^{146}Nd/^{144}Nd = 0.7219$. Analysis of NBS SRM 987 yielded $^{87}Sr/^{86}Sr = 0.710237 \pm 12$ (2 s.d., $n = 50$). Analysis of La Jolla Nd standard yielded $^{143}Nd/^{144}Nd = 0.511849 \pm 10$ (2 s.d., $n = 16$). Two analyses of rock standard BHVO-1 gave an average $^{87}Sr/^{86}Sr$ of 0.703474 and $^{143}Nd/^{144}Nd$ of 0.512973. Twenty analyses of NBS SRM 981 gave $^{206}Pb/^{204}Pb = 16.935 \pm 9$, $^{207}Pb/^{204}Pb = 15.486 \pm 12$, $^{208}Pb/^{204}Pb = 36.689 \pm 35$ corrected for 0.13‰ fractionation per mass unit, and have an estimated accuracy of 0.03% (2 s.d.) per mass unit.

The Kerimasi data indicate an overall homogeneous source with uniform Sr and Nd isotopic compositions (0.70391–0.70406, 0.51272–0.51273). Samples from Wasaki Peninsula display a small variation in $^{143}Nd/^{144}Nd$ ratios ranging from 0.51265 to 0.51275 (Table 1, Fig. 2) and also a small variation in $^{87}Sr/^{86}Sr$ ratios between 0.70381 and 0.70417 (Table 1, Fig. 2). The samples from the Homa Mountain area show an extreme variation in $^{143}Nd/^{144}Nd$ ratios from 0.51249 to 0.51283 (Table 1, Fig. 2) and in $^{87}Sr/^{86}Sr$ ratios (0.70327 to 0.70502, Table 1, Fig. 2).

Measured $^{206}Pb/^{204}Pb$ ratios range between 18.72 and 20.41, $^{207}Pb/^{204}Pb$ ratios between 15.52 and 15.78, and $^{208}Pb/^{204}Pb$ ratios between 39.22 and 40.47 (Table 1). Age corrections are negligible assuming average $^{238}U/^{204}Pb$ ratios as given by Nelson et al. (1988) and Simonetti and Bell (1994b). Only calculations with extreme $^{238}U/^{204}Pb$ ratios of >100 lead to significant shifts in $^{206}Pb/^{204}Pb$ ratios, and calculations with high Th/U ratios result in significant shifts in $^{208}Pb/^{204}Pb$ ratios when correcting for in-situ decay (Nelson et al., 1988).

In the Pb isotope plots, the measured ratios of samples from Lake Victoria and Kerimasi form arrays with positive correlations (Fig. 3). In a $^{207}Pb/^{204}Pb$ versus $^{206}Pb/^{204}Pb$ diagram the data plot on and parallel to the Northern Hemisphere Reference Line (NHRL; Hart, 1984), with $^{207}Pb/^{204}Pb$ ratios shifted towards slightly higher values for a given $^{206}Pb/^{204}Pb$ ratio (Fig. 3a). In the $^{208}Pb/^{204}Pb$ versus $^{206}Pb/^{204}Pb$ diagram a trend oblique to the NHRL is observed with $\Delta 8/4$ values (Hart, 1984) increasing with decreasing $^{206}Pb/^{204}Pb$ ratios. Analogous to the Sr and Nd isotope systematics, the largest variation in Pb isotope ratios is shown by the samples from the Homa Mountain area ($^{206}Pb/^{204}Pb = 18.718$–$20.414$, Table 1, Fig. 3). The most radiogenic Pb isotope ratios with only small variations are displayed by the samples from

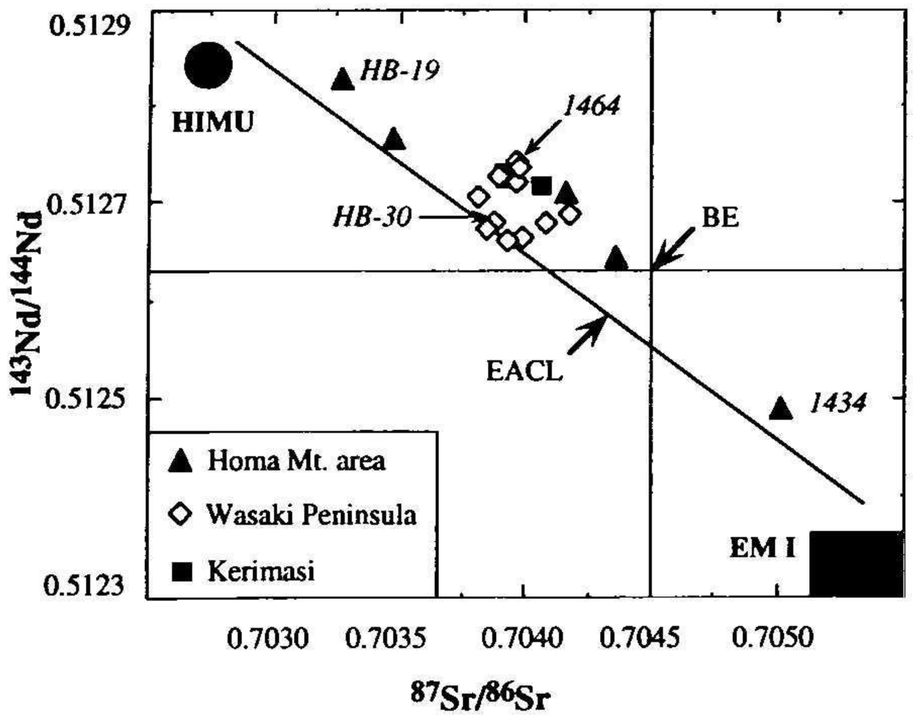

Fig. 2. Diagram of $^{143}Nd/^{144}Nd$ versus $^{87}Sr/^{86}Sr$ showing measured ratios of carbonatite, ijolite, and melilitite samples from the Homa Mountain area, Wasaki Peninsula (Lake Victoria, Kenya), and Kerimasi (Tanzania). The East African Carbonatite Line (EACL) of Bell and Blenkinsop (1987) is also shown. *BE* = bulk earth value. Fields for HIMU and EM I components shown according to Hart et al. (1986).

Kerimasi ($^{206}Pb/^{204}Pb$ = 20.648–20.817, Table 1, Fig. 3), whereas the samples from Wasaki Peninsula have intermediate Pb isotope ratios ($^{206}Pb/^{204}Pb$ = 19.272–20.343, Table 1, Fig. 3).

4. Discussion and conclusions

4.1. Compositions of the mantle sources

The Nd–Sr and the Pb–Pb data arrays indicate that carbonatites, ijolites, and melilitites from Lake Victoria and Kerimasi were generated from an isotopically heterogeneous mantle. The linearity of the arrays in the Sr–Nd and Pb–Pb isotope plots suggests binary mixing processes. As set out in Section 1, carbonatite sources are commonly interpreted in the context of mantle components identified in oceanic basalts (HIMU, DMM, EM I, EM II). Similarly, the Sr–Nd isotopic compositions of the studied samples as a whole may be interpreted in terms of mixing of two endmember components: a HIMU-type component with high $^{143}Nd/^{144}Nd$ ratios and low $^{87}Sr/^{86}Sr$ ratios and an EM I-type component with low $^{143}Nd/^{144}Nd$ ratios and high $^{87}Sr/^{86}Sr$ ratios (Figs. 2 and 5). The enriched (EM I) endmember is not well-defined by our data due to the position of

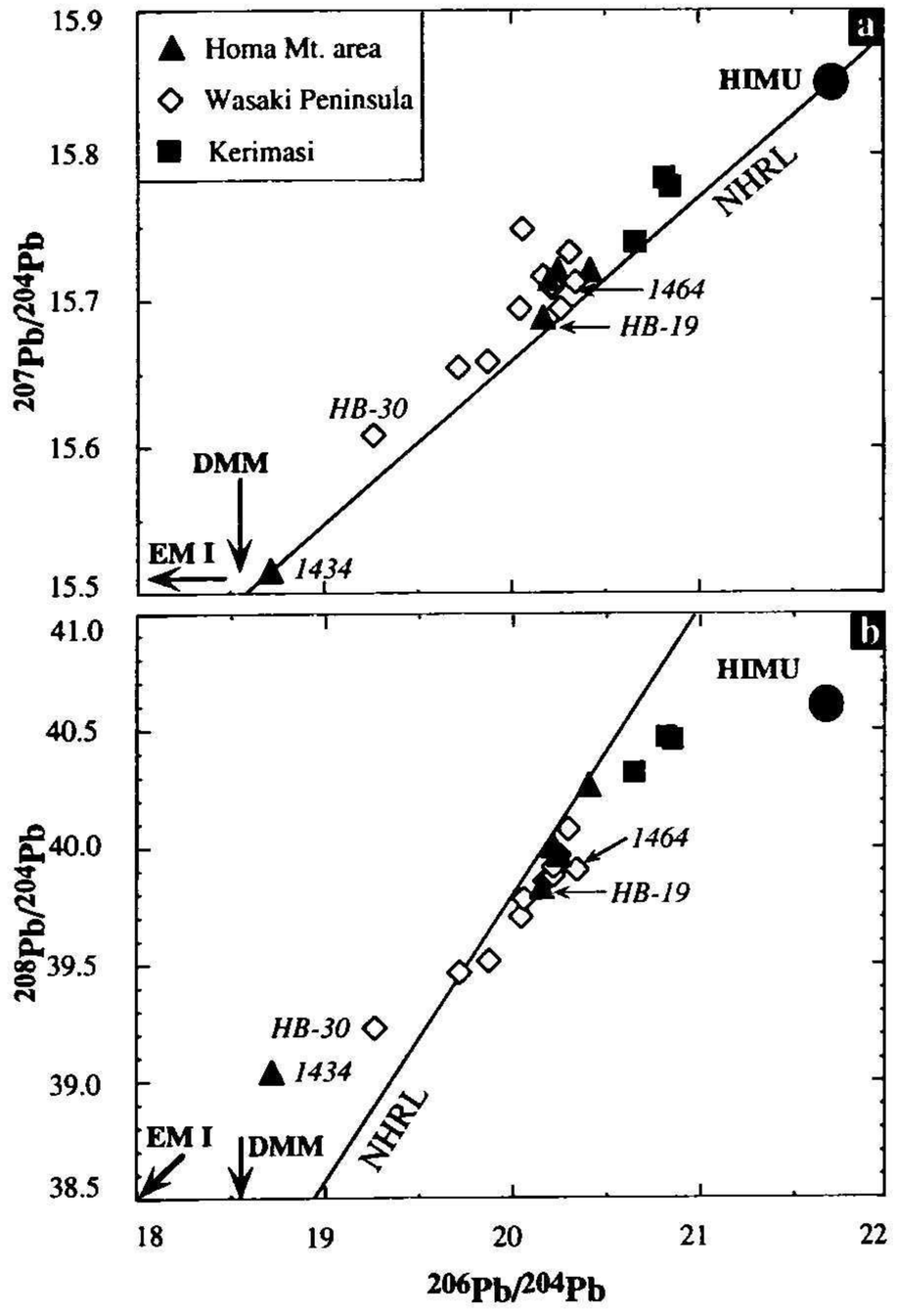

Fig. 3. Diagrams of $^{207}Pb/^{204}Pb$ versus $^{206}Pb/^{204}Pb$ (a) and $^{208}Pb/^{204}Pb$ versus $^{206}Pb/^{204}Pb$ (b) showing measured ratios of carbonatite, ijolite, and melilitite samples from the Homa Mountain area, Wasaki Peninsula (Lake Victoria, Kenya), and Kerimasi (Tanzania). Also shown is the Northern Hemisphere Reference Line (*NHRL*) of Hart (1984). Fields for HIMU, DMM and EM I components shown according to Hart et al. (1986).

most data points within the depleted quadrant of the Sr–Nd isotope diagram. HIMU–EM I binary mixing for the samples as a whole is also suggested by a data trend oblique to the NHRL in the $^{208}Pb/^{204}Pb$ versus $^{206}Pb/^{204}Pb$ diagram (Fig. 3b).

However, a closer examination of the data reveals that the observed variations in Sr, Nd and Pb isotopic compositions are not produced by binary mixing of HIMU and EM I components. In the Sr–Nd isotope diagram, the variations within the three carbonatite areas are diverse. Only the data for Homa Mountain area are consistent with binary mixing of HIMU and EM I components. The spread displayed by samples

from Kerimasi is too small for any correlation to be recognised and the data field for Wasaki Peninsula shows no linear trend. Additionally, the position of data points in the $^{207}Pb/^{204}Pb$ versus $^{206}Pb/^{204}Pb$ diagram is more consistent with involvement of a DMM-type component rather than EM I as the sample with the least radiogenic Pb (1434) plots on the NHRL close to DMM (Fig. 3a).

A further feature not in line with binary HIMU–EM I mixing is the lack of consistent endmember compositions. If this process were a realistic model for the carbonatites studied here, the samples closest to the two endmember compositions should be the same in all isotope diagrams. The sample similar to HIMU composition should have the lowest $^{87}Sr/^{86}Sr$ ratios, the highest $^{143}Nd/^{144}Nd$ ratios, and the most radiogenic Pb isotope ratios. On the contrary, the sample approximating EM I composition should display the highest $^{87}Sr/^{86}Sr$ ratios, the lowest $^{143}Nd/^{144}Nd$ ratios, and the least radiogenic Pb isotope ratios. This is not the case for the carbonatites studied here. Samples from Kerimasi, for example, have an intermediate composition in the $^{143}Nd/^{144}Nd$ versus $^{87}Sr/^{86}Sr$ plot while they display the most radiogenic Pb isotope ratios. A similar observation can be made for the samples approximating HIMU (HB-19) and the EM I (1434) compositions in the Sr–Nd isotope plot (Fig. 2). Sample 1434 also plots close to EM I in both Pb isotope diagrams (Fig. 3), but sample HB-19 displays an intermediate Pb isotope composition unlike HIMU. This inconsistent behaviour is also evident from the $^{87}Sr/^{86}Sr$ versus $^{206}Pb/^{204}Pb$ (Fig. 4a) and the $^{143}Nd/^{144}Nd$ versus $^{206}Pb/^{204}Pb$ diagram (Fig. 4b). The data points form irregular clusters instead of linear arrays and thus no trend is developed.

When applied to the individual carbonatite areas (Kerimasi, Homa Mountain area, Wasaki Peninsula), a binary HIMU–EM I mixing model also fails to explain the respective data arrays. The samples from Kerimasi are similar in all isotope diagrams, so that no trend is recognisable (Figs. 2–4). Additional data from Kerimasi (Paslick et al., 1995; see Section 4.2., Figs. 5–7) show that this is not due to our small data base. The data for Wasaki Peninsula show trends consistent with binary HIMU–EM I mixing in the Pb–Pb diagrams, but not in the Sr–Nd isotope plot (compare samples HB-30 and 1464 in Figs. 2–4).

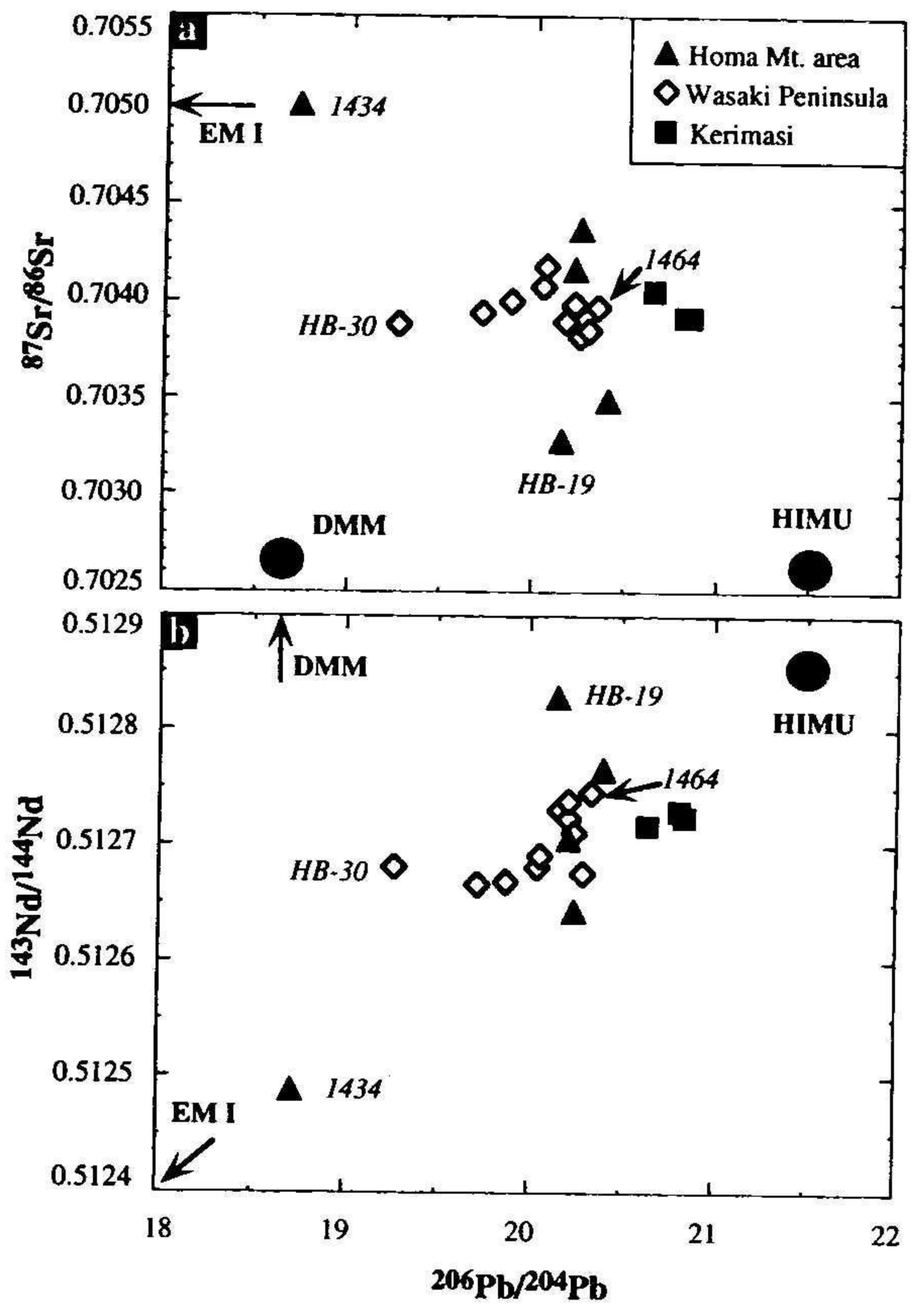

Fig. 4. Diagrams of $^{87}Sr/^{86}Sr$ versus $^{206}Pb/^{204}Pb$ (a) and $^{143}Nd/^{144}Nd$ versus $^{206}Pb/^{204}Pb$ (b) showing measured ratios of carbonatite, ijolite, and melilitite samples from the Homa Mountain area, Wasaki Peninsula (Lake Victoria, Kenya), and Kerimasi (Tanzania). Fields for HIMU, DMM and EM I components shown according to Hart et al. (1986).

The samples from Homa Mountain area suggest a HIMU–EM I trend on the $^{143}Nd/^{144}Nd$ versus $^{87}Sr/^{86}Sr$ plot (Fig. 2). Nevertheless, as argued above, there is no consistency in endmembers (compare samples 1434 and HB-19 in Figs. 2–4). Additionally, the vertical trends displayed by the Homa Mountain data in the Sr–Pb and Nd–Pb diagrams (Fig. 4) suggest decoupling of the U–Pb from the Rb–Sr and Sm–Nd systems rather than binary mixing.

In summary, neither the data as a whole nor those for individual complexes can be explained by binary mixing between HIMU and EM I or any other components identified in oceanic island basalts. Instead, the data suggest distinct mantle sources for the three areas that are each isotopically heterogeneous

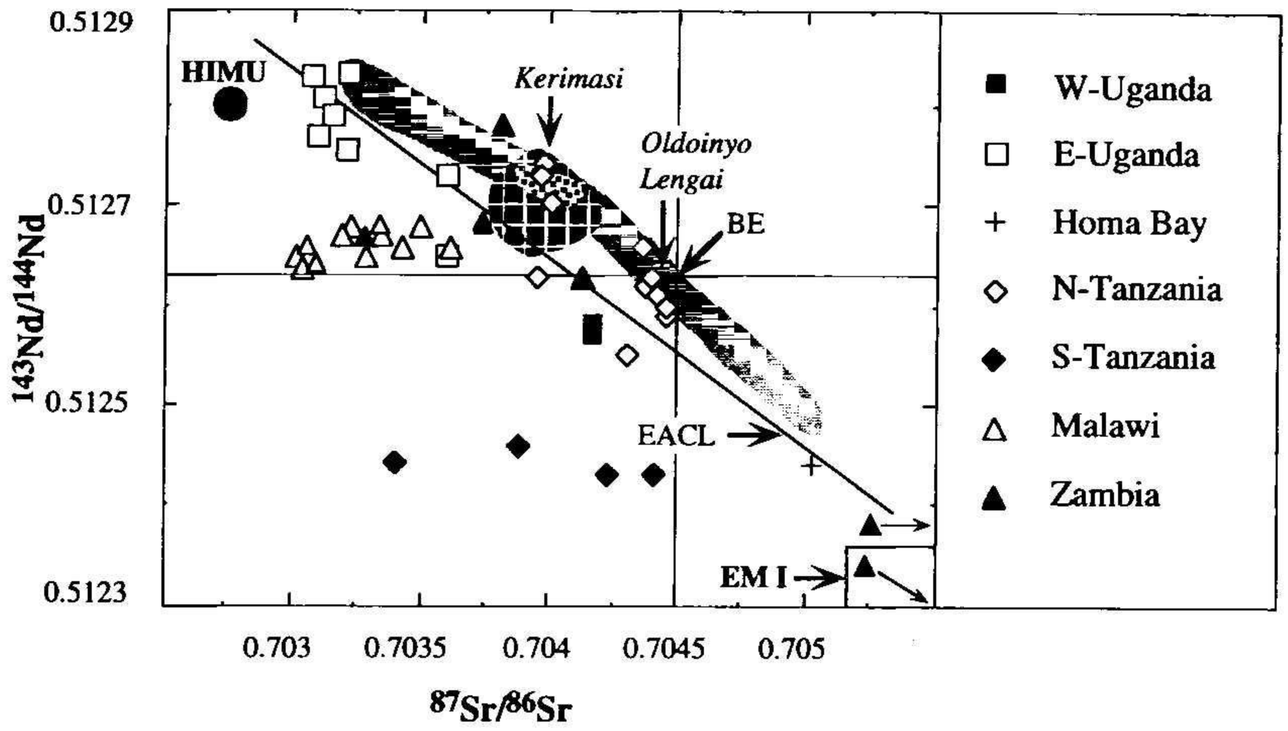

Fig. 5. Diagram of $^{143}Nd/^{144}Nd$ versus $^{87}Sr/^{86}Sr$ showing data from previous studies on East African carbonatites as listed in Table 2. For samples younger than 40 Ma (W-Uganda, E-Uganda, Homa Bay, N-Tanzania), measured ratios are plotted. For samples older than 40 Ma (S-Tanzania, Malawi, Zambia), initial ratios are shown. Two samples from Zambia (filled triangles) plot outside the diagram to the lower right side. Also shown for comparison are the data fields of this study: Kerimasi (stippled), Wasaki Peninsula (checkered), and Homa Bay (grey). The East African Carbonatite Line (*EACL*) of Bell and Blenkinsop (1987) and the bulk earth value (*BE*) are also shown. For further explanation see text. Fields for HIMU and EM I components shown according to Hart et al. (1986).

to different degrees. Along with the fact that carbonatite magmatism in general is volumetrically very restricted, these observations suggest the existence of small-scale mantle sources and mixing processes between components that vary in composition and space.

4.2. Comparison with other East African carbonatites

Numerous Sr, Nd, and Pb isotope data on East African carbonatites and related rocks have been published. Although there is a considerable range in age and tectonic setting between individual complexes (Fig. 1, Table 2) it has been concluded that the Sr, Nd, and Pb isotope systematics of East African carbonatites younger than 200 Ma studied so far are consistent with mixing of HIMU and EM I mantle components (Bell and Blenkinsop, 1987; Bell, 1994; Tilton and Bell, 1994; Bell and Dawson, 1995). Therefore, data for carbonatites older than those studied here, but younger than 200 Ma, and data for carbonatites from other parts of the East African Rift system have been included in the following discussion. All data used for comparison have been compiled in Table 2 and are shown in Figs. 5–7. Comparison of the cited isotope standard values shows these to coincide within error limits (see footnotes to Tables 1 and 2).

Carbonatites have been grouped according to their tectonic and geographic situations (Figs. 1, 5–7, Table 2). This gross oversimplification is adapted for the sake of clarity in Figs. 5–7. For carbonatites younger than 40 Ma, age corrections for Sr, Nd, and Pb isotope ratios are negligible assuming average Rb/Sr, Sm/Nd, U/Pb, and Th/U ratios (Nelson et al., 1988; Ziegler, 1992; Simonetti and Bell, 1994a,b; Paslick et al., 1995). For these samples, measured ratios are shown in Figs. 5–7. For carbonatites older than 40 Ma, initial isotope ratios are plotted in the respective diagrams.

The carbonatites of Kerimasi, Oldoinyo Lengai, and Shombole volcanoes are referred to as 'N-Tanzania'. They are situated next to the western fault scarp within the Kenya Rift (eastern branch of the East African Rift) and are of Neogene age (Dawson, 1992). The carbonatite complexes of Bukusu, Tororo, Sukulu, and Napak (E-Uganda) are located on the eastern shoulder of the Kenya Rift and display mineral ages ranging between 7 and 32 Ma (Simonetti and Bell, 1993, 1994a). Carbonatites from Kalyango and Rusekere crop out in the Fort Portal area (W-Uganda) on the eastern shoulder of the Albert Rift. Volcanic activity occurred about 4–6

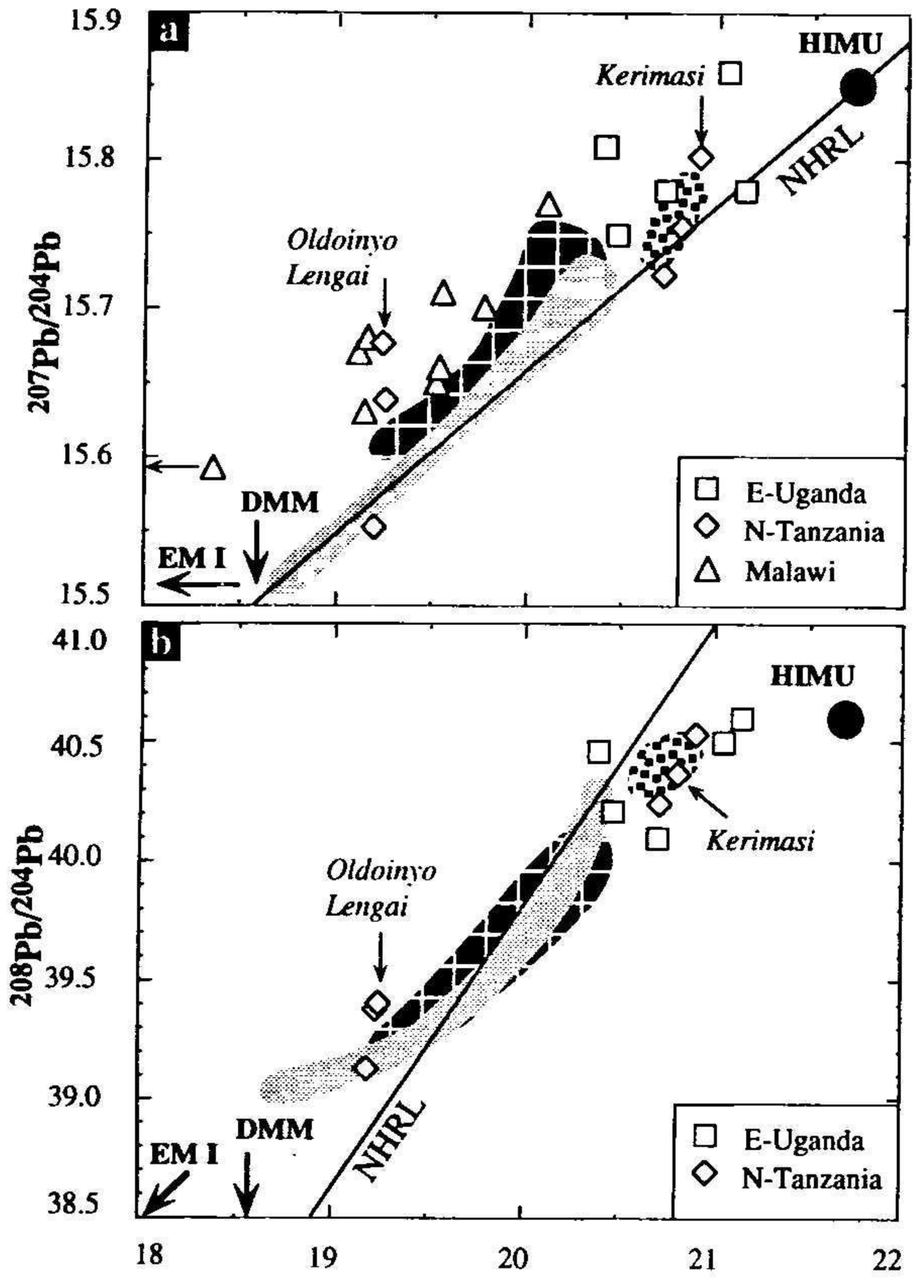

Fig. 6. Diagrams of $^{207}Pb/^{204}Pb$ versus $^{206}Pb/^{204}Pb$ (a) and $^{208}Pb/^{204}Pb$ versus $^{206}Pb/^{204}Pb$ (b) showing data from previous studies on East African carbonatites as listed in Table 2. For samples younger than 40 Ma (E-Uganda, N-Tanzania), measured ratios are plotted. For samples older than 40 Ma (Malawi), initial ratios are shown. One sample from Malawi plots outside both diagrams to the left side. Also shown for comparison are the data fields of this study: Kerimasi (stippled), Wasaki Peninsula (checkered), and Homa Bay (grey). *NHRL* is the Northern Hemisphere Reference Line of Hart (1984). For further explanation see text. Fields for HIMU, DMM and EM I components shown according to Hart et al. (1986).

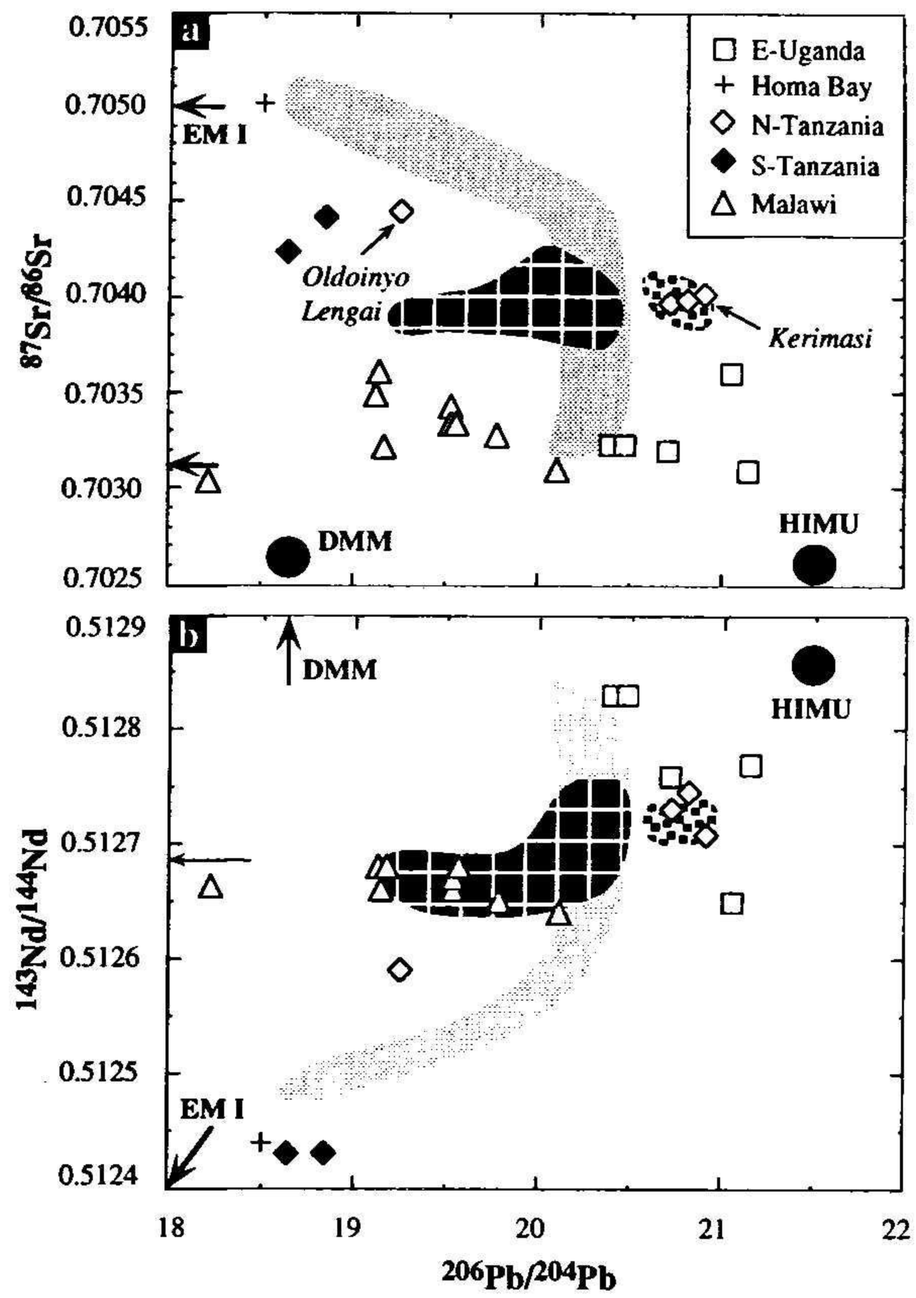

Fig. 7. Diagrams of $^{87}Sr/^{86}Sr$ versus $^{206}Pb/^{204}Pb$ (a) and $^{143}Nd/^{144}Nd$ versus $^{206}Pb/^{204}Pb$ (b) showing data from previous studies on East African carbonatites as listed in Table 2. For samples younger than 40 Ma (E-Uganda, Homa Bay, N-Tanzania), measured ratios are plotted. For samples from Malawi (126 Ma), initial ratios are shown. For samples from S-Tanzania (Panda Hill, 113 Ma), Sr and Nd initial ratios were calculated from measured ratios given by Bell and Blenkinsop (1987) with average Sm/Nd and Rb/Sr ratios as given by Ziegler (1992) for Panda Hill carbonatites. $^{206}Pb/^{204}Pb$ ratios were taken from Fig. 6 of Tilton and Bell (1994) and may represent either measured or initial ratios. Also shown for comparison are the data fields of this study: Kerimasi (stippled), Wasaki Peninsula (checkered), and Homa Bay (grey). For further explanation see text. Fields for HIMU, DMM and EM I components shown according to Hart et al. (1986).

ka ago (Barker and Nixon, 1989). Panda Hill and Sengeri (S-Tanzania) are located at the junction of the eastern and the western rift branch south of the Tanzania Craton. A K–Ar age of 113 Ma has been reported by Snelling (1965) for Panda Hill. The carbonatites from Chilwa Island, Lake Chilwa, and from Kangankunde are part of the Chilwa Alkaline Province (Malawi) and related to the east–west trending fault system of the Zambesi Rift (Simonetti and Bell, 1994b). An age of 126 Ma is cited by these authors and by Ziegler (1992). The carbonatite complexes of Kaluwe and Chasweta form part of the Rufunsa Province (Zambia) located at the triple junction of the Luangwa and Zambesi rift systems. They display K–Ar mineral ages of 101–113 Ma (Ziegler, 1992).

Table 2
Compilation of Sr–Nd–Pb isotopic data for East African carbonatites

Region	Complex	Age (Ma)	Ref.	$^{87}Sr/^{86}Sr$	$^{143}Nd/^{144}Nd$	$^{206}Pb/^{204}Pb$	$^{207}Pb/^{204}Pb$	$^{208}Pb/^{204}Pb$
W-Uganda	Kalyango	0	BB87	0.70417	0.51257			
	Rusekere	0	BB87	0.70417	0.51258			
E-Uganda	Bukusu	26–32	BB87	0.70315	0.51279			
	Bukusu	26–32	BB87	0.70307	0.51283			
	Sukulu	26–32	BB87	0.70312	0.51281			
	Tororo	26–32	BB87	0.70360	0.51273			
	Tororo	26–32	N88	0.70360	0.51267	21.068	15.865	41.112
	Sukulu	26–32	N88	0.70311	0.51280	21.154	15.781	40.646
	Napak	7–30	N88	0.70320	0.51278	20.719	15.780	40.379
	Napak	7–30	SB94a	0.70323	0.51283	20.40	15.81	40.46
	Napak	7–30	SB94a	0.70323	0.51283	20.47	15.75	40.21
Kenya	Homa Bay	13	BB87	0.70502	0.51244	18.50		
N-Tanzania	Old Leng	0	BB87	0.70442	0.51261			
	Old Leng	0	BB87	0.70445	0.51259	19.25		
	Old Leng	0	KK90	0.70437	0.51262			
	Old Leng	0	KK90	0.70439	0.51263			
	Old Leng	0	D95			19.245	15.676	39.365
	Old Leng	0	D95			19.261	15.637	39.396
	Old Leng	0	D95			19.200	15.552	39.125
	Kerimasi	0.5	P95	0.703975	0.512744	20.809	15.754	40.361
	Kerimasi	0.5	P95	0.703967	0.512730	20.712	15.722	40.236
	Kerimasi	0.5	P95	0.704003	0.512706	20.907	15.801	40.516
	Shombole	2	BP91	0.70395	0.51263			
	Shombole	2	BP91	0.70430	0.51255			
	Shombole	2	BP91	0.70436	0.51266			
	Shombole	2	BP91	0.70445	0.51260			
S-Tanzania	Panda Hill	113	BB87	0.70442	0.51243	18.85		
	Sengeri	113	BB87	0.70423	0.51243	18.65		
	Panda Hill	113	Z92	0.703874	0.512458			
	Panda Hill	113	Z92	0.703406	0.512442			
Malawi	Kangank	126	N88	0.7031	0.51264	20.11	15.78	
	Kangank	126	Z92	0.703016	0.512650			
	Kangank	126	Z92	0.703067	0.512660			
	Kangank	126	Z92	0.703033	0.512637			
	Chilwa	126	SB94b	0.70328	0.51265	19.78	15.70	
	Chilwa	126	SB94b	0.70334	0.51267	19.54	15.66	
	Chilwa	126	SB94b	0.70349	0.51268	19.13	15.67	
	Chilwa	126	SB94b	0.70322	0.51268	19.18	15.68	
	Chilwa	126	SB94b	0.70319	0.51267	17.31	15.59	
	Chilwa	126	SB94b	0.70334	0.51268	19.57	15.71	
	Chilwa	126	SB94b	0.70342	0.51266	19.53	15.65	
	Chilwa	126	SB94b	0.70361	0.51266	19.15	15.63	
Zambia	Kaluwe	113	Z92	0.703284	0.512668			
	Kaluwe	113	Z92	0.704121	0.512630			
	Kaluwe	113	Z92	0.703740	0.512683			
	Chasweta	113	Z92	0.707738	0.512392			
	Chasweta	113	Z92	0.705717				
	Chasweta	113	Z92	0.706337	0.512228			
	Chasweta	113	Z92	0.703810	0.512781			

Sr–Nd data are available for all the carbonatite occurrences mentioned above. Samples of 40 Ma and younger as a whole form an array on the $^{143}Nd/^{144}Nd$ versus $^{87}Sr/^{86}Sr$ diagram that is similar to the one defined by our samples (Fig. 5). This correlation (including older samples from S-Tanzania) has been interpreted as an isotopically heterogeneous mantle source resulting from mixing of a HIMU and an EM I component (Bell and Blenkinsop, 1987; Bell, 1994; Bell and Dawson, 1995). However, the isotope data for individual carbonatite areas younger than 40 Ma do not follow the EACL or any other HIMU–EM I mixing line. An exception may be the data array for E-Uganda. However, this field contains data from four individual carbonatite centres and thus the isotopic variations and trends for each centre are not constrained. On the other hand, it is noteworthy that data points for the neighbouring Oldoinyo Lengai and Kerimasi volcanoes (N-Tanzania) define separate fields on the $^{143}Nd/^{144}Nd$ versus $^{87}Sr/^{86}Sr$ diagram. Thus, binary mixing of a HIMU and an EM I component as a process common to the sources of East African carbonatites younger than 40 Ma is not clearly evident from the Sr–Nd data. The data arrays can be better explained by assuming distinct sources for individual carbonatite areas or complexes that have no common mixing endmembers.

A similar conclusion can also be drawn from the Pb data. In a $^{207}Pb/^{204}Pb$ versus $^{206}Pb/^{204}Pb$ diagram, data for carbonatites younger than 40 Ma show a trend parallel to and above the NHRL, similar to our data (Fig. 6a). As for our study, the trends displayed by the data for individual carbonatite areas (E-Uganda and N-Tanzania) are not in line with the general trend. Again, it is noteworthy that Kerimasi and Oldoinyo Lengai (N-Tanzania) display entirely different Pb isotope ratios. A similar relationship is shown in the $^{208}Pb/^{204}Pb$ versus $^{206}Pb/^{204}Pb$ diagram (Fig. 6b). A trend oblique to the NHRL, as displayed by our data, is also shown by the samples from E-Uganda and N-Tanzania as a whole, but the individual trends do not mimic the general correlation. The lack of consistent HIMU–EM I mixing trends can also be depicted from the $^{87}Sr/^{86}Sr$ and $^{143}Nd/^{144}Nd$ versus $^{206}Pb/^{204}Pb$ diagrams (Fig. 7). Again, individual carbonatite areas define distinct trends.

The older East African carbonatites (40–126 Ma) cannot easily be compared to young carbonatites (<40 Ma) in terms of mantle sources. Mantle source compositions for carbonatites younger than 40 Ma are represented by the isotopic compositions of the samples as in-situ decay is negligible. Contrary, the present-day compositions of the mantle sources for older carbonatites are not directly accessible due to significant in-situ decay. They must be modeled from the initial isotope compositions of the samples assuming mother/daughter isotope ratios for the mantle source. Calculations of this kind bear vast uncertainties as the actual Rb/Sr, Sm/Nd, U/Pb, and Th/U ratios of the mantle sources are not known. Therefore, the locations of the present-day mantle source fields for the older carbonatites on the isotope diagrams are not known and cannot be compared with those of carbonatites younger than 40 Ma. It is only evident that each of the older carbonatite areas has a distinct source. This emerges from the distinct fields formed by initial Sr–Nd isotope ratios of individual areas (S-Tanzania, Malawi, Zambia) in the Sr–Nd isotope plot (Fig. 5).

Footnote to Table 2

Isotope ratios given as measured ratios for samples younger than 40 Ma and as initial ratios for older samples. BB: Bell and Blenkinsop (1987), initial Sr and Nd isotope ratios for Panda Hill and Sengeri calculated with averages of $^{87}Rb/^{86}Sr$ and $^{147}Sm/^{144}Nd$ ratios as given by Ziegler (1992) for Panda Hill, $^{206}Pb/^{204}Pb$ ratios taken from Fig. 6 of Tilton and Bell (1994); N88: Nelson et al. (1988), $^{143}Nd/^{144}Nd$ calculated with ϵ_{Nd} values given in Table 2; SB94a: Simonetti and Bell (1994a); KK90: Keller and Krafft (1990); D95: Dawson et al. (1995); P95: Paslick et al. (1995); BP91: Bell and Peterson (1991); Z92: Ziegler (1992); initial Sr and Nd isotope ratios calculated using $^{87}Rb/^{86}Sr$ and $^{147}Sm/^{144}Nd$ ratios as given in Tables 2–3; SB94b: Simonetti and Bell (1994b), initial isotope ratios as given by the authors. $\lambda_{Rb} = 1.42 \times 10^{-11}$, $\lambda_{Sm} = 6.54 \times 10^{-12}$. In all cited studies, $^{87}Sr/^{86}Sr$ ratios are normalized to $^{86}Sr/^{88}Sr = 0.1194$, $^{143}Nd/^{144}Nd$ ratios to $^{146}Nd/^{144}Nd = 0.7219$, except for N88 ($^{146}Nd/^{142}Nd = 0.63151$). Standard values given by the authors: La Jolla: 0.51186 ± 2 (BB87, BP91, SB94a,b), 0.511845 ± 9 (P95); BCR1: 0.511833 ± 20 (N88), 0.51266 ± 2 (SB94a,b); NBS SRM 987: 0.71023 ± 3 (BB87), 0.71022 ± 4 (N88), 0.71025 ± 2 (SB94a,b), 0.710247 ± 15 (P95); Eimer and Amend: 0.70808 ± 3 (BB87, BP91), 0.70800 ± 3 (N88); NBS SRM 981 ($^{206}Pb/^{204}Pb$): 16.927 ± 9 (N88), NBS SRM 981 ($^{207}Pb/^{204}Pb$): 15.486 ± 13 (N88), NBS SRM 981 ($^{208}Pb/^{204}Pb$): 36.668 ± 44 (N88). For further explanations see Section 4.2.

In summary, Sr, Nd, and Pb isotope compositions of East African carbonatites display a wide range in Sr, Nd, and Pb isotope compositions. Although a crude HIMU–EM I correlation may be depicted from the Sr–Nd (Figs. 2 and 5) and the Pb–Pb isotope plots (Figs. 3 and 6), such a trend is seen neither in the Sr–Pb and Nd–Pb isotope relationships (Figs. 4 and 7) nor in the trends displayed by single carbonatite areas on all isotope plots. These observations are consistent with diverse mantle sources for East African carbonatites that are not produced by mixing of common endmembers.

4.3. Location of the mantle sources of East African carbonatites

The isotope data imply small-scale heterogeneities in the mantle sources for East African Rift carbonatites, a conclusion that has already been drawn in other studies on East African carbonatites (Bell and Blenkinsop, 1987; Bell and Dawson, 1995) and has also been proposed for East African nephelinites on the basis of isotope data (Simonetti and Bell, 1993, 1994a, 1995; Bell and Simonetti, 1996). Several mixing scenarios were proposed to explain the isotopic variations in the carbonatite sources, e.g., mixing between asthenospheric melts and ancient enriched lithospheric mantle, between lower crust and depleted mantle, or between enriched asthenosphere and depleted subcontinental mantle (Bell and Dawson, 1995), or plume–lithosphere interaction combined with different degrees of partial melting (Bell and Simonetti, 1996). We suggest that East African Rift carbonatites could be generated entirely in the lithospheric mantle. A similar conclusion has been drawn by Paslick et al. (1995) for young volcanics of northern Tanzania, including carbonatites from Kerimasi. A major role of the lithosphere for the sources of nephelinites and carbonatites has also been invoked by Bell and Simonetti (1996).

Isotopic evidence argues against significant involvement of the convecting asthenospheric mantle. If this were the case, at least one mixing endmember with consistent Sr–Nd–Pb isotopic composition as for example DMM should be recognisable. This is clearly not the case for East African Rift carbonatites. Involvement of plume material, commonly related to a HIMU-type component, also appears unlikely. In cases where a mantle plume and/or asthenosphere have significantly contributed to an East African Rift mantle source, consistent mixing trends and endmembers in isotope and trace-element compositions were found (Class et al., 1994; Volker et al., 1995). For East African Rift carbonatites, the irregular isotopic trends for each of the areas under investigation argue against contributions from any mantle reservoirs that are continuously available.

Isotopic evidence argues in favour of a heterogeneous lithospheric mantle as carbonatite source region. The data arrays for East African Rift carbonatites as a whole reveal two important features. (1) In the $^{208}Pb/^{204}Pb$ versus $^{206}Pb/^{204}Pb$ diagram (Fig. 3b and Fig. 6b), a trend towards compositions with high $^{208}Pb/^{204}Pb$ and low $^{206}Pb/^{204}Pb$ ratios, due to high Th/U ratios, can be recognised. Reservoirs with high Th/U ratios are known to exist in the lithospheric mantle and to result from time-integrated Th enrichment by metasomatism (Williams et al., 1992; Carlson and Irving, 1994). (2) In the Sr–Pb and Nd–Pb correlation diagrams, there is a trend towards a composition that shows HIMU features for Pb, but intermediate $^{87}Sr/^{86}Sr$ and $^{143}Nd/^{144}Nd$ ratios. Such compositions are not reflected by oceanic island basalts. Similar isotopic characteristics have previously been described by Paslick et al. (1995) for young volcanics from Tanzania. Paslick et al. (1995) were able to model the isotope and trace-element spectrum of the Tanzanian volcanics assuming a lithospheric mantle enriched with a 2 Ga OIB source. Isotopic heterogeneities in East African carbonatites could thus be explained by assuming generation from a heterogeneous lithospheric mantle containing small domains variably enriched at different times to different degrees.

This conclusion is in line with xenolith evidence from the East African Rift. Geochemical and mineralogical studies on peridotite xenoliths from Pello Hill, Olmani, and Lashaine (all northern Tanzania) document both depletion and metasomatic enrichment in the lithospheric mantle (Dawson et al., 1970; Reid et al., 1975; Jones et al., 1982; Dawson and Smith, 1988; Rudnick et al., 1993). Isotope data for these xenoliths reveal strong heterogeneity, indicating ancient enrichment processes (Cohen et al., 1984), although some of the lithospheric mantle heterogeneity seems to result from younger, short-lived

and small-scaled metasomatism with asthenospheric chemical imprint (Dawson and Smith, 1988; Rudnick et al., 1993).

A major role of the lithosphere is further supported by the existence of a relationship between isotope data and tectonic setting of the carbonatite areas. The distinct isotopic trends displayed by each of these areas most likely reflect the different tectonic settings (see Section 4.2) and thus contributions from different portions of a heterogeneous lithospheric mantle.

A lithospheric origin is also consistent with experimental results, requiring unusual mantle compositions for the generation of carbonatites. The results show carbonatite magmas to be derived from carbonated phlogopite and/or amphibole-bearing peridotites (Wallace and Green, 1988; Eggler, 1989; Wyllie, 1989; Dalton and Wood, 1993; Sweeny, 1994). The very small volumes of carbonatites compared to the amount of silicate mantle-derived rocks in the East African Rift (and in general) indicate these mantle compositions to occur only in small portions of the mantle. Carbonated phlogopite and/or amphibole-bearing peridotites can be in equilibrium with carbonatite melts at depths between 60 and 120 km (Wallace and Green, 1988; Thibaut et al., 1992; White and Wyllie, 1992; Sweeny, 1994), indicating that generation of carbonatites entirely in the lithosphere is possible in regions of very thick lithosphere. Estimates of lithospheric thickness, deduced from geothermobarometric studies on mantle xenoliths (Henjes-Kunst and Altherr, 1992) range from 75 km beneath Marsabit (N-Kenya) to 115 km beneath Chyulu Hills (S-Kenya) to >145 km beneath Lashaine (N-Tanzania).

Acknowledgements

The authors wish to thank Jörg Keller for providing samples TK-12, TK-14, TK-26, HB-19, HO-1, HO-4, and HB-30 and for critical comments on a first draft of the manuscript. We would also like to thank Rainer Altherr for discussion and helpful comments. A. Simonetti and H.G. Stosch are thanked for constructive and helpful reviews. Financial support by the Deutsche Forschungsgemeinschaft within the Special Research Program 'Stress and stress release in the lithosphere' (University of Karlsruhe, SFB 108, C2) is gratefully acknowledged. This is SFB 108 contribution No. 583.

References

Achauer, U., the KRISP Teleseismic Working Group, 1994. New ideas on the Kenya Rift based on the inversion of the combined dataset of the 1985 and 1989/90 seismic tomography experiments. Tectonophysics, 236: 305–329.

Bailey, D.K., 1993. Carbonatite magmas. J. Geol. Soc. London 150, 637–651.

Baker, B.H., 1987. Outline of the petrology of the Kenya rift alkaline province. In: Fitton, J.G., Upton, B.J.G. (Eds.), Alkaline Igneous Rocks. Blackwell, London, pp. 293–311.

Baker, B.H., Williams, L.A.J., Miller, J.A., Fitch, F.J., 1970. Sequence and chronology of the Kenya Rift volcanics. Tectonophysics 11, 191–215.

Barker, D.S., Nixon, P.H., 1989. High-Ca, low-alkali carbonatite volcanism at Fort Portal, Uganda. Contrib. Mineral. Petrol. 103, 166–177.

Bell, K., 1994. Carbonatites and mantle evolution: a review. Mineral. Mag. 58A, 69–70.

Bell, K., Blenkinsop, J., 1987. Nd and Sr isotopic compositions of East African carbonatites: implications for mantle heterogeneity. Geology 15, 99–102.

Bell, K., Blenkinsop. J., 1989. Neodymium and strontium isotope geochemistry of carbonatites. In: Bell, K. (Ed.), Carbonatites. Unwin Hyman, Boston, pp. 278–300.

Bell, K., Dawson, B., 1995. Nd and Sr isotope systematics of the active carbonatite volcano, Oldoinyo Lengai. In: Bell, K., Keller, J. (Eds.), Carbonatite Volcanism. Springer, Berlin, pp. 100–112.

Bell, K., Peterson, T., 1991. Nd and Sr isotope systematics of Shombole volcano, East Africa, and the links between nephelinites, phonolites, and carbonatites. Geology 19, 582–585.

Bell, K., Simonetti, A., 1996. Nd, Pb and Sr isotope systematics from Oldoinyo Lengai carbonatite volcano (Tanzania): carbonatite magmatism and lithosphere–plume interaction. J. Conf. Abstr. 1, 56.

Carlson, R.W., Irving, A.J., 1994. Depletion and enrichment history of subcontinental lithospheric mantle: an Os, Sr, Nd and Pb isotopic study of ultramafic xenoliths from the northwestern Wyoming Craton. Earth Planet. Sci. Lett. 126, 457–472.

Class, C., Altherr, R., Volker, F., Eberz, G., McCulloch, T.M., 1994. Geochemistry of Pliocene to Quaternary alkali basalts from the Huri Hills, northern Kenya. Chem. Geol. 113, 1–22.

Cohen, R.S., O'Nions, R.K., Dawson, J.B., 1984. Isotope geochemistry of xenoliths from East Africa: implications for development of mantle reservoirs and their interaction. Earth Planet. Sci. Lett. 68, 209–220.

Dalton, J.A., Wood, B.J., 1993. The compositions of primary carbonatite melts and their evolution through wallrock reaction in the mantle. Earth Planet. Sci. Lett. 119, 511–525.

Dawson, J.B., 1992. Neogene tectonics and volcanicity in the North Tanzania sector of the Gregory Rift Valley: contrasts with the Kenya sector. Tectonophysics 204, 81–92.

Dawson, J.B., Smith, J.V., 1988. Metasomatized and veined upper-mantle xenoliths from Pello Hill, Tanzania: evidence for anomalously-light mantle beneath the Tanzanian sector of the East African Rift Valley. Contrib. Mineral. Petrol. 100, 510–527.

Dawson, J.B., Powell, D.G., Reid, A.M., 1970. Ultrabasic xenoliths and lava from the Lashaine volcano, Northern Tanzania. J. Petrol. 11, 519–548.

Dawson, B.J., Pinkereton, H., Norton, G.E., Pyle, D.M., Browning, P., Jackson, D., Fallick, A.E., 1995. Petrology and geochemistry of Oldoinyo Lengai lavas extruded in November 1988: Magma source, ascent and crystallization. In: Bell, K., Keller, J. (Eds.), Carbonatite Volcanism. Springer, Berlin, pp. 47–69.

Ebinger, C.J., Bechtel, T.D., Forsyth, D.W., Bowin, C.O., 1989. Effective elastic thickness beneath the East African and Afar plateaus and dynamic compensation of uplift. J. Geophys. Res. 94, 2883–2901.

Eggler, D.H., 1989. Carbonatites, primary melts, and mantle dynamics. In: Bell, K. (Ed.), Carbonatites. Unwin Hyman, Boston, pp. 561–579.

Hart, S.R., 1984. A large-scale isotope anomaly in the Southern Hemisphere mantle. Nature 309, 753–757.

Hart, S.R., Gerlach, D.C., White, W.M., 1986. A possible new Sr–Nd–Pb mantle array and consequences for mantle mixing. Geochim. Cosmochim. Acta 50, 1551–1557.

Hegner, E., Roddick, C.R., Fortier, S.M., Hulbert, L., 1995. Nd, Sr, Pb, Ar, and O isotopic systematics of Sturgeon Lake kimberlite, Saskatchewan, Canada: constraints on emplacement age, alteration, and source composition. Contrib. Mineral. Petrol. 120, 212–222.

Henjes-Kunst, F., Altherr, R., 1992. Metamorphic petrology of xenoliths from Kenya and Northern Tanzania and implications for geotherms and lithospheric structures. J. Petrol. 33, 1125–1156.

Hoernle, K.A., Tilton, G.R., 1991. Sr–Nd–Pb isotope data for Fuertaventura (Canary Islands) basal complex and subaerial volcanics: applications to magma genesis and evolution. Schweiz. Mineral. Petrogr. Mitt. 71, 3–18.

Jones, A.P., Smith, J.V., Dawson, J.B., 1982. Glasses in mantle xenoliths from Olmani, Tanzania. J. Geol. 91, 167–178.

Keller, J., Krafft, M., 1990. Effusive natrocarbonatite activity, Oldoinyo Lengai, June 1988. Bull. Volcanol. 52, 629–645.

Keller, J., Spettel, B., 1995. Trace element composition and petrogenesis of natrocarbonatites. In: Bell, K., Keller, J. (Eds.), Carbonatite Volcanism. Springer, Berlin, pp. 70–86.

Kwon, S.T., Tilton, G.R., Gruenenfelder, M., 1989. Lead isotope relationships in carbonatites and alkalic complexes: an overview. In: Bell, K. (Ed.), Carbonatites. Unwin Hyman, Boston, pp. 360–387.

Lancelot, J.R., Allègre, C.J., 1974. Origin of carbonatitic magma in the light of the Pb–U–Th isotope system. Earth Planet. Sci. Lett. 22, 133–238.

Le Bas, M.J., 1977. Carbonatite–Nephelinite Volcanism. Wiley, Chichester, 347 pp.

Le Bas, M.J., 1987. Nephelinites and carbonatites. In: Fitton, J.G., Upton, B.G.J. (Eds.), Alkaline Igneous Rocks. Blackwell, Oxford, pp. 53–84.

McCall, G.H.J., 1958. Geology of the Gwasi area. Geol. Surv. Kenya Rep., 45, 88 pp.

McDougall, I., Watkins, R.T., 1988. Potassium–argon ages of volcanic rocks from the northeast of Lake Turkana, northern Kenya. Geol. Mag. 125, 15–23.

Nelson, D.R., Chivas, A.R., Chappell, B.W., McCulloch, M.T., 1988. Geochemical and isotopic systematics in carbonatites and implications for the evolution of ocean-island sources. Geochim. Cosmochim. Acta 52, 1–17.

Paslick, C., Halliday, A., James, D., Dawson, B., 1995. Enrichment of the continental lithosphere by OIB melts: isotopic evidence from the volcanic province of northern Tanzania. Earth Planet. Sci. Lett. 130, 109–126.

Perry, F.V., Baldrige, W.F., DePaolo, D.J., 1987. Role of asthenosphere and lithosphere in the genesis of late Cenozoic basaltic rocks from the Rio Grande Rift and adjacent regions of the southwestern United States. J. Geophys. Res. 92, 9193–9213.

Peterson, T.D., 1989. Peralkaline nephelinites. I. Comparative petrology of Shombole and Oldoinyo Lengai, East Africa. Contrib. Mineral. Petrol. 101, 458–478.

Reid, A.M., Donaldson, C.H., Brown, R.W., Ridley, W.I., Dawson, B.J., 1975. Mineral chemistry of peridotite xenoliths from the Lashaine volcano, Tanzania. Phys. Chem. Earth 9, 525–543.

Rudnick, R.L., McDonough, W.F., Chappell, B., 1993. Carbonatite metasomatism in the Northern Tanzanian mantle: petrographic and geochemical characteristics. Earth Planet. Sci. Lett. 114, 463–475.

Shackleton, R.M., 1993. Tectonics of the Mozambique Belt in East Africa. In: Prichard, H.M., Alabaster, T., Harris, N.B.W., Neary, C.R. (Eds.), Magmatic Processes and Plate Tectonics. Geol. Soc. Spec. Publ. 76, 345–362.

Simonetti, A., Bell, K., 1993. Isotopic disequilibrium in clinopyroxenes from nephelinitic lavas, Napak Volcano, eastern Uganda. Geology 21, 243–246.

Simonetti, A., Bell, K., 1994a. Nd, Pb and Sr isotopic data from the Napak carbonatite–nephelinite centre, eastern Uganda: an example of open-system crystal fractionation. Contrib. Mineral. Petrol. 115, 356–366.

Simonetti, A., Bell, K., 1994b. Isotopic and geochemical investigation of the Chilwa Island Carbonatite Complex, Malawi: evidence for a depleted mantle source region, liquid immiscibility, and open system behaviour. J. Petrol. 35, 1597–1621.

Simonetti, A., Bell, K., 1995. Nd, Pb and Sr isotopic data from the Mount Elgon volcano, eastern Uganda–western Kenya: implications for the origin and evolution of nephelinite lavas. Lithos 36, 141–153.

Simonetti, A., Bell, K., Viladkar, S.G., 1995. Isotopic data from the Amba Dongar Carbonatite Complex, west-central India: evidence for an enriched mantle source. Chem. Geol. 122, 185–198.

Smith, M., 1994. Stratigraphic and structural constraints on mechanisms of active rifting in the Gregory Rift, Kenya. Tectonophysics 236, 3–22.

Smith, M., Mosley, P., 1993. Crustal heterogeneity and basement

influence on the development of the Kenya Rift, East Africa. Tectonics 12, 591–606.

Snelling, N.J., 1965. Age determination on three African carbonatites. Nature 205, 491.

Sweeny, R.J., 1994. Carbonatite melt compositions in the earth's mantle. Earth Planet. Sci. Lett. 128, 259–270.

Thibaut, Y., Edgar, A.D., Lloyd, F.E., 1992. Experimental investigation of melts from a carbonated phlogopite lherzolite: implications for metasomatism in the continental lithospheric mantle. Am. Mineral. 77, 784–794.

Tilton, G.R., Bell, K., 1994. Sr–Nd–Pb isotope relationships in Late Archean carbonatites and alkalic complexes: applications to the geochemical evolution of Archean mantle. Geochim. Cosmochim. Acta 58, 3145–3154.

Treiman, A.H., 1989. Carbonatite magma: properties and processes. In: Bell, K. (Ed.), Carbonatites. Unwin Hyman, Boston, pp. 89–104.

Volker, F., Altherr, R., McCulloch, T.M., 1995. Geochemistry and Sr–Nd–Pb isotopic evolution of the Marsabit volcanic field, NE Kenya: constraints on magma genesis in the mantle beneath the Kenya Rift. Chem. Geol. (submitted).

Wallace, M.A., Green, D.H., 1988. An experimental determination of primary carbonatite composition. Nature 335, 343–346.

White, B.S., Wyllie, P.J., 1992. Solidus reactions in synthetic peridotite–H_2O–CO_2 from 20–30 kbar, with applications to melting and metasomatism. J. Volcanol. Geotherm. Res. 50, 117–130.

Williams, R.W., Gill, J.B., Bruland, K.W., 1986. Ra–Th disequilibria systematics: timescale of carbonatite magma formation at Oldoinyo Lengai volcano, Tanzania. Geochim. Cosmochim. Acta 50, 1249–1259.

Williams, R.W., Collerson, K.D., Gill, J.B., Deniel, C., 1992. High Th/U ratios in subcontinental lithospheric mantle: mass spectrometric measurement of Th isotopes in Gaussberg lamproites. Earth Planet. Sci. Lett. 111, 257–268.

Woolley, A.R., 1989. The spatial and temporal distribution of carbonatites. In: Bell, K. (Ed.), Carbonatites. Unwin Hyman, London, pp. 15–37.

Wyllie, P.J., 1989. Origin of carbonatites: evidence from phase equilibrium studies. In: Bell, K. (Ed.), Carbonatites. Unwin Hyman, Boston, pp. 500–545.

Ziegler, U.R.F., 1992. Preliminary results of geochemistry, Sm–Nd and Rb–Sr studies of post-Karoo carbonatite complexes in Southern Africa. Schweiz. Mineral. Petrogr. Mitt. 72, 135–142.

Zindler, A., Hart, S., 1986. Chemical geodynamics. Ann. Rev. Earth. Planet. Sci. 14, 493–571.